Supplementary Material

Text S1. Traditional Gradient-based Front Identification Method

The gradient thresholding method is the traditional ocean front detection method, which is mainly based on the gradient of some quantity (typically SST or SSH) exceeding some pre-defined thresholds, and then identifies the points exceeding the threshold as fronts. We use this method to establish the SAF dataset for training and validation of the SAFNet.

The gradient method used in this study is the classical Sobel operator method (Kittler, 1983). The algorithm calculated the SST and SSH gradient at each pixel. First, a Gaussian filter was adopted to make the SST map and SSH map smooth. A Gaussian filter is a linear smoothing filter that can remove isolated noise and increase the width of the edges. The equation of Gaussian filter is as follows:

$$g_\sigma(m,n) = \frac{1}{\sqrt{2\pi\sigma^2}} e^{-\frac{m^2+n^2}{2\sigma^2}} \cdot f(m,n) \tag{1}$$

where $f(m,n)$ represents the pixel value at the (m,n) position, $g_\sigma(m,n)$ represents the value of each point after Gaussian filtering, and σ represents the standard deviation. In fact, Equation (1) actually means a Gaussian matrix convolves with each pixel and its neighborhood. Then, the Sobel operator that consists of two 3 ×3 convolution masks G_x and G_y are used to compute the gradient vector. As for $G_x = [-1\ 0\ 1;\ -2\ 0\ 2;\ -1\ 0\ 1]$ and $G_y = [-1-2-1;\ 0\ 0\ 0;\ 1\ 2\ 1]$, they convolve with each pixel and approximate the first-order derivative $g_x(m,n)$ and $g_y(m,n)$, respectively. The final gradient magnitude of each pixel at (m,n) can be computed with Equation (2) below:

$$G(m,n) = \sqrt{g_x(m,n)^2 + g_y(m,n)^2} \tag{2}$$

The gradient magnitude of each pixel is calculated by Equation (2) to obtain the gradient magnitude map. According to the pre-defined gradient threshold, the pixels in the gradient magnitude map that are greater than the threshold are set to 1 to represent the front, and the other pixels are set to 0 to represent the non-front.

Text S2. SAF Dataset

Figure S1 shows two samples of the SAF dataset. We arbitrarily select two days from the daily SST and SSH data from 2010 to 2019 as two samples of the SAF dataset for presentation. Figures S1 (A) - (D) show the SST and SSH distributions on January 1 and August 1, 2016. Firstly, we use the gradient-based front identification method (Text S1) to automatically calculate the corresponding SST and SSH gradient magnitude maps from the SST and SSH data, as shown in Figure S1 (E) - (H). Figures S1 (I) - (L) display the SST front (yellow zone) and SSH front (green zone) identified from the gradient magnitude map using the pre-defined threshold, and the selected threshold is consistent with former studies (Chapman, 2017, Wang et al., 2021). Finally, the union of the two kinds of fronts is used to represent the SAF in the ideal state, which fuses the thermal and dynamic characteristics, and take this as the ground truth of the SAF [Figure S1 (M), (N)]. We take the daily ground truth of the SAF from

2010 to 2018 as the training set, which contains 3287 samples. The ground truth of 2019 is used as the validation set, which contains a total of 365 samples.

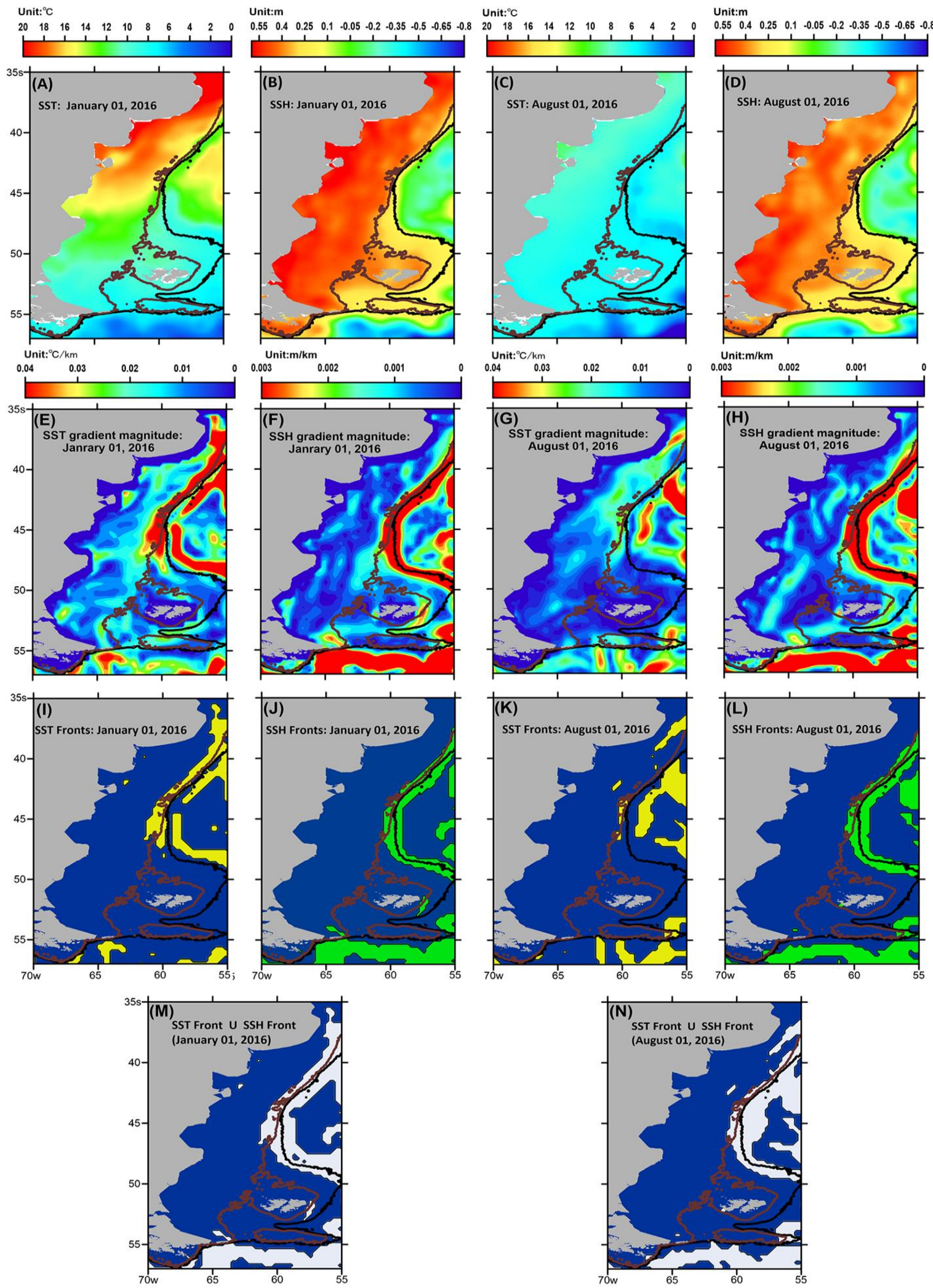

Figure S1. Two samples of the SAF dataset. (A)-(D) display the SST and SSH distributions over the Southwestern Atlantic in January 1 and August 1, 2016. (E)-(H) show the corresponding gradient magnitude maps for these two days. The SST fronts (yellow zones) and SSH fronts (green zones) are displayed in (I)-(L), which are obtained from the corresponding gradient magnitude map by the threshold. (M) and (N) represent the ground truth of the SAF (white zones) on January 1 and August 1, 2016. The brown and black solid contours are 200m and 1000m isobaths, respectively.

Text S3. Evaluation Metrics

To objectively evaluate the detection accuracy of SAFNet and other models for SAF, four classical evaluation metrics, Intersection over Union (IoU), Accuracy, Precision, and Recall were used in the comparison experiments.

$$IoU = \frac{TP}{FP + TP + FN} \tag{3}$$

$$Accuracy = \frac{TP + TN}{TP + TN + FP + FN} \tag{4}$$

$$Precision = \frac{TP}{TP + FP} \tag{5}$$

$$Recall = \frac{TP}{TP + FN} \tag{6}$$

where TP, FP, FN, and TN represent the number of true positive, false positive, false negative, and true negative ocean front pixels, respectively. In our experiments, true positive represents the number of pixels that are identified as fronts in both the detection results and the ground truth. False positive denotes the number of pixels that are identified as non-fronts in the ground truth and as fronts in the detection results. False negative represents the number of pixels identified as fronts in the ground truth and as non-fronts in the results. True negative denotes the number of pixels are identified as non-fronts in both the ground truth and results. The higher the above four evaluation metrics represent the higher accuracy of the frontal detection results.

Table S1 Performances of SAFNet and other methods

Model / Metrics	SAFNet	DFN+D-LinkNet	DFN+LinkNet
IoU	**97.11%**	89.55%	87.12%
Accuracy	**99.45%**	97.05%	96.22%
Precision	**98.82%**	94.90%	93.62%
Recall	**98.63%**	94.30%	92.50%

Text S4. Ablation Experiment

In this study, since the convolutional block attention module (CBAM) and dilated convolution layers (DCLs) are integrated into SAFNet to improve the detection accuracy of SAF, ablation experiments are needed to analyze the contribution of CBAM and DCLs to the high-precision detection of SAF. The ablation experiments in this study were designed to remove CBAM and DCLs to test their effect on the accuracy of detection results. We performed ablation experiments on SAFNet on the validation set using the evaluation metrics presented in Text S3. Table S2 shows the accuracy indicator of ablation experiments. To visually present the results of the ablation experiments, Figure S2 shows the comparison of the detection results between the ground truth of 4 days arbitrarily selected from the validation set and SAFNet with different modules removed. It can be clearly found that when the model does not integrate CBAM and DCLs, the accuracy is significantly reduced.

Table S2 Ablation experiments on validation set

Model / Metrics	SAFNet	$\text{SAFNet}_{\text{without CBAM}}$	$\text{SAFNet}_{\text{without CBAM \& DCLs}}$
IoU	**97.11%**	94.07%	91.37%
Accuracy	**99.45%**	96.33%	95.68%
Precision	**98.82%**	94.93%	92.83%
Recall	**98.63%**	97.27%	96.18%

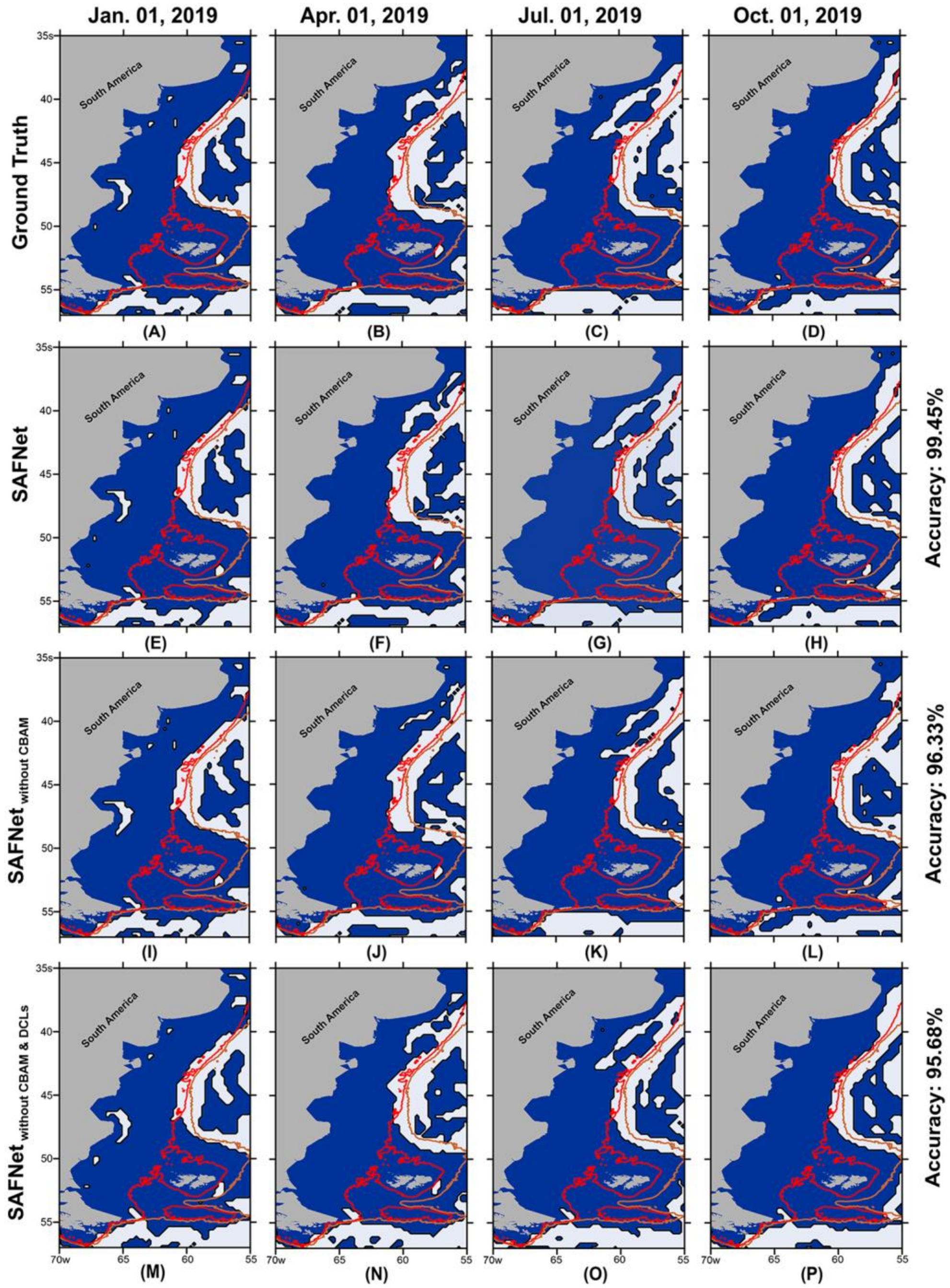

Figure S2. Results of ablation experiments on CBAM and DCLs. The white zone represents the SAF and the blue area is the non-frontal zone. Red and brown solid contours are 200m and 1000m isobaths, respectively.

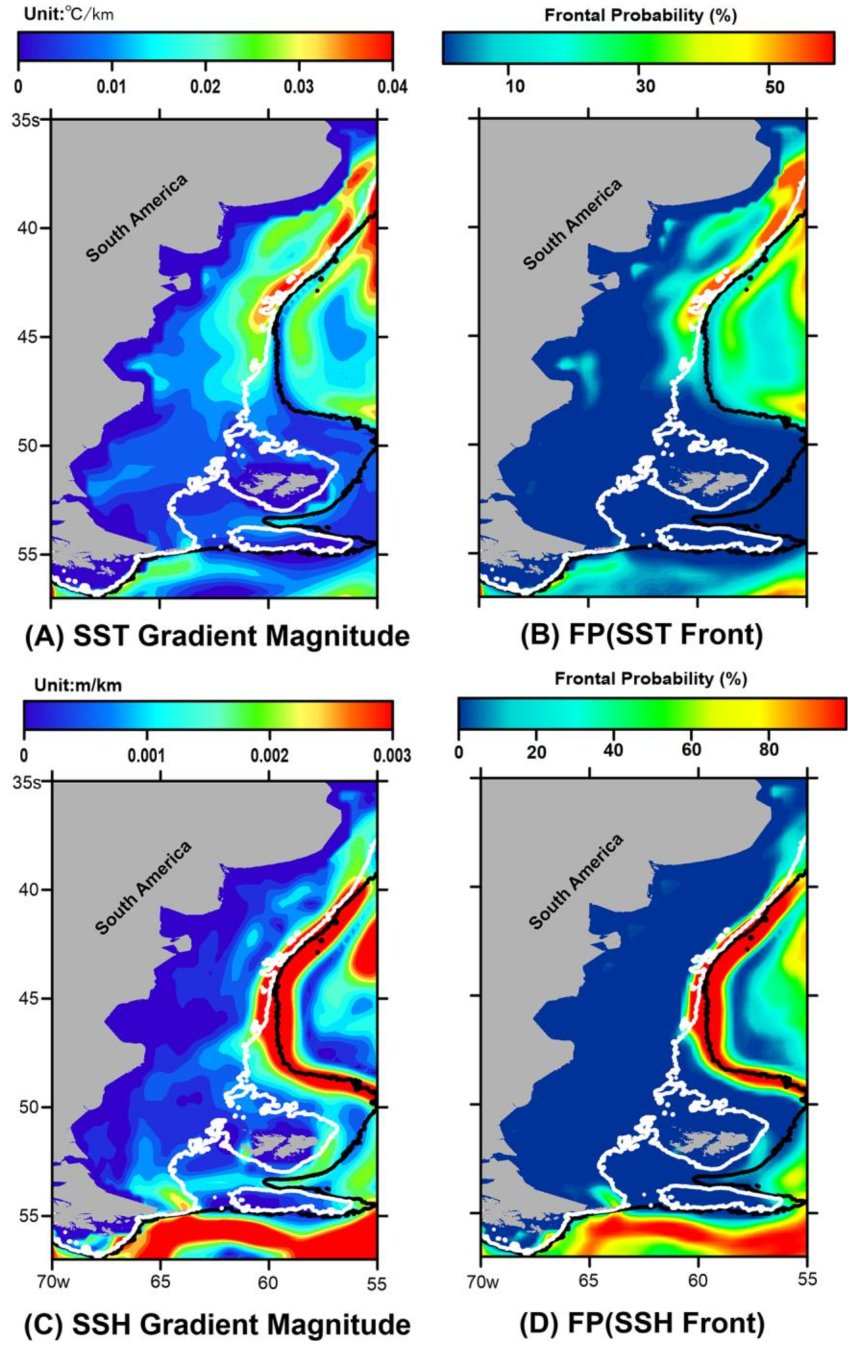

Figure S3. The overall mean of SST and SSH gradient magnitude for 2010-2019 (left), and the overall mean of SST FP and SSH FP for 2010-2019 (right). The white and black solid contours are 200m and 1000m isobaths, respectively.

Text S5. Comparison of Seasonal Distributions of Southwestern Atlantic Thermal and Dynamic Fronts

Figure S4 (A)-(D) presents the seasonal mean SST distributions in the Southwestern Atlantic (SA) for 2010-2019. We know that SST distribution has obvious seasonal differences compared to SSH. SA is bounded by the 200m isobath, and the temperature difference between the two sides is most obvious in summer and decreases in winter. The main reason for this seasonal difference stems from the increasing surface cooling effects in winter, which makes the SSTs of the Falkland Current (a strong cold current) and the South American shelf water uniform. This phenomenon also leads to the thermal front (derived from the SST data) disappears in winter, and the front phenomenon is significantly weaker than that in summer [Figure S4 (E)-(H)]. Obviously, there are seasonal limitations to detecting the SAF only by SST.

The SSH distribution reflects the dynamic process of SA. The Falkland Current intrudes into the shelf water of South America along the 1000m isobath all year around, so the SSH distribution of SA is bounded by the 1000m isobath, and the difference between the two sides is obvious and stable [Figure S4 (I)-(L)]. The SSH gradient magnitude maps are shown in Figure S4 (M)-(P). Compared with the thermal front, the Southwestern Atlantic dynamic front (derived from the SSH data) has a more stable spatiotemporal distribution, which can overcome the seasonal limitations of SST. However, in the shelf waters (within the 200m isobaths), the dynamic front is weaker than the thermal front. This is mainly because the dynamic mechanism of the shelf waters is relatively stable so the dynamic characteristics of the SAF are not obvious. However, due to the invasion of the Falkland Current, the shelf water has obvious temperature differences, so the thermal characteristics of the SAF are obvious. Therefore, SAF is detected only by SSH, the detection results cannot fully reflect the spatial distribution of SAF.

In summary, neither the thermal front detected by SST nor the dynamic front detected by SSH can fully and accurately represent the SAF. The thermal front disappears in winter, so it has seasonal limitations. Compared with the thermal front, the dynamic front is more stable in seasonal distribution and can overcome the seasonal limitations of the thermal front. The dynamic front cannot reflect the front distribution in shelf waters, while the thermal front is mainly distributed in shelf water, which can compensate for the absence of dynamic front. Therefore, SAF has prominent thermal and dynamic characteristics, and the thermal front and dynamic front are reflections of the thermal and dynamic characteristics of SAF, respectively. To realize the accurate detection of SAF, it is necessary to fuse its thermal and dynamic characteristics, which requires the fusion of multi-source remote sensing data.

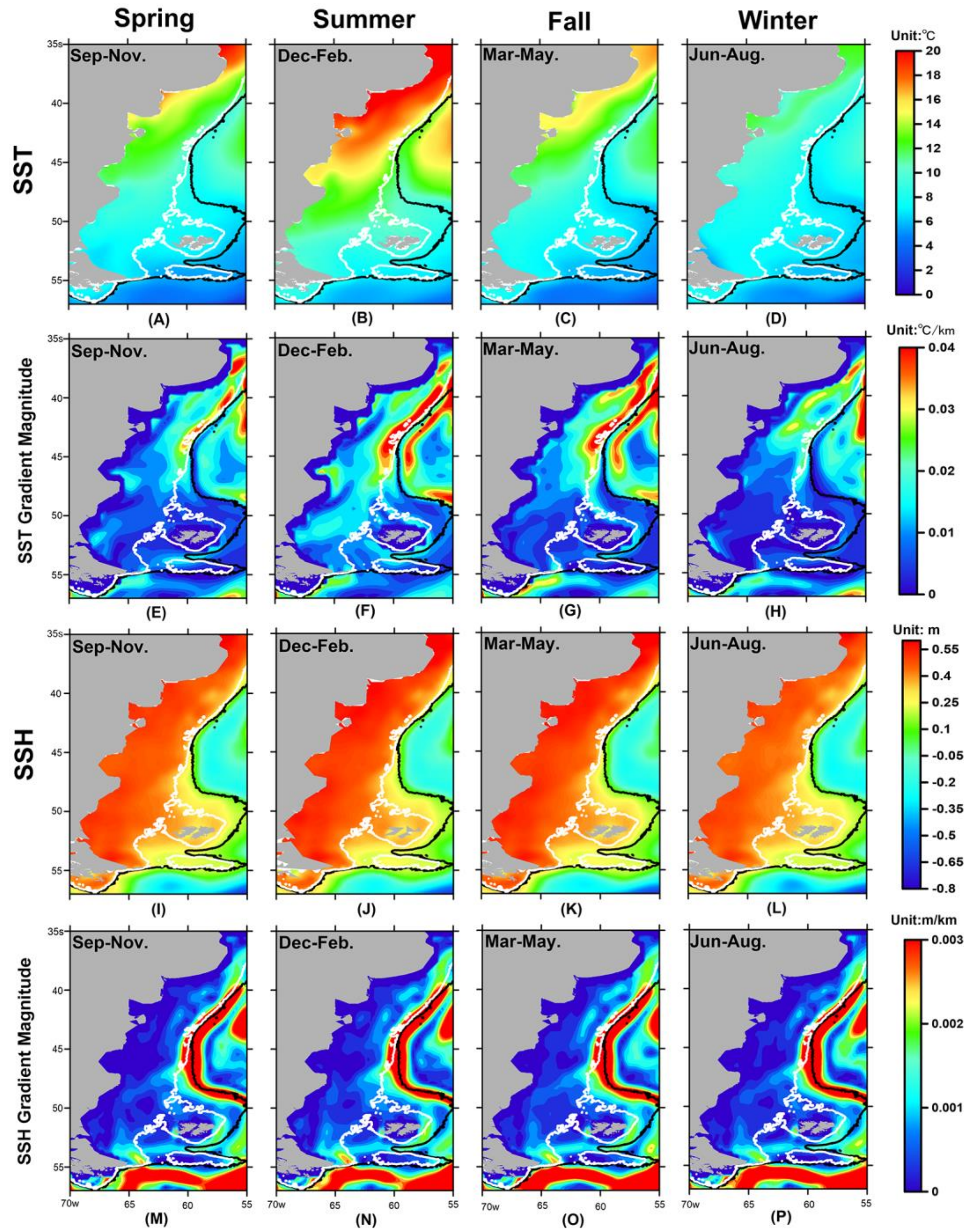

Figure S4. Seasonal distribution of Southwestern Atlantic thermal and dynamical fronts. (A)-(D) are the seasonal mean SSTs for 2010-2019. (E)-(H) are SST gradient magnitude maps, which used to represent the seasonal distribution of the Southwestern Atlantic thermal front. The seasonal mean SSHs for 2010-2019 are shown in (I)-(L), and their corresponding SSH gradient magnitude maps are presented in (M)-(P). The SSH gradient magnitude map can represent the distribution of the dynamic front. The white and black solid contours are 200m and 1000m isobaths, respectively.

References

CHAPMAN, C. C. 2017. New Perspectives on Frontal Variability in the Southern Ocean. *Journal of Physical Oceanography,* 47**,** 1151-1168.

KITTLER, J. 1983. On the accuracy of the Sobel edge detector. *Image and Vision Computing,* 1**,** 37-42.

WANG, Z., CHEN, G., HAN, Y., MA, C. & LV, M. 2021. Southwestern Atlantic Ocean Fronts Detected from Satellite-Derived SST and Chlorophyll. *Remote Sensing,* 13.